Spectroscopic evidence for a charge-density-wave condensate in a charge-ordered manganite: Observation of a collective excitation mode in $Pr_{0.7}Ca_{0.3}MnO_3$ by using THz time-domain spectroscopy

Noriaki Kida and Masayoshi Tonouchi
Research Center for Superconductor Photonics, Osaka University, 2-1 Yamadaoka, Suita, Osaka 565-0871, Japan and CREST, Japan Science & Technology Corporation (JST), 2-1 Yamadaoka, Suita, Osaka 565-0871, Japan
(Received 11 March 2002; revised manuscript received 22 April 2002; published 24 June 2002)

THz time-domain spectroscopy was used to directly probe the low-energy (0.5–5 meV) electrodynamics of the charge-ordered manganite $Pr_{0.7}Ca_{0.3}MnO_3$. We revealed the existence of a finite peak structure around 2–3 meV well below the charge gap ~300 meV. In analogy to the low-energy optical properties of the well-studied low-dimensional materials, we attributed this observed structure to the collective excitation mode arising from the charge-density-wave condensate. This finding provides the importance role of the quasi-one-dimensional nature of the charge and orbital ordering in $Pr_{0.7}Ca_{0.3}MnO_3$.

DOI: 10.1103/PhysRevB.66.024401 PACS number(s): 75.30.Vn, 71.45.Lr, 72.15.Nj, 73.20.Mf

I. INTRODUCTION

The tendency toward for the formation of charge ordering is a common characteristic of transition metal oxides with perovskite structure including high-temperature superconducting cuprates and colossal magnetoresistive manganites.[1,2] In particular, various kinds of manganites with the doping level x of 1/2 show charge-exchange (CE)-type charge ordering,[2,3] in which Mn^{3+} and Mn^{4+} ions by the ratio of 1:1 regularly distribute in the underlying lattice below the charge and orbital ordering temperature $T_{CO/OO}$ [Fig. 1(a)]. Such a real-space charge ordering is characterized by a single-particle excitation across the charge gap 2Δ. Using the light of frequency ω, the single-particle excitation spectrum of the charge-ordered (CO) manganites have been extensively investigated in recent years;[4–9] for example, Okimoto *et al.* identified $2\Delta \sim 300$ meV of $Pr_{0.6}Ca_{0.4}MnO_3$ by using polarized reflectivity measurements and clarified that the electronic structure is dramatically reconstructed on the order of electron volts by varying temperature T and magnetic field H (Refs. 5 and 6). Using transmission measurements, Calvani *et al.* found that $2\Delta(T)$ of $La_{1-x}Ca_xMnO_3$ with $x=0.5$ and 0.67 can be well described by the Bardeen-Cooper-Schrieffer (BCS) relation.[7]

Another important viewpoint is the collective nature of e_g carriers including the orbital degree of freedom, which is thought to have a great impact on extraordinary properties of the manganites, i.e., colossal magnetoresistance (CMR).[10] The conspicuous examples are recent findings of the ''orbiton,'' a new elementary excitation of the orbital-ordered state observed in $LaMnO_3$,[11] and of the ''charge stripes,'' a new periodic form composed of a pairing of diagonal Mn^{3+} with Mn^{4+} observed in $La_{1-x}Ca_xMnO_3$ ($x \geqslant 1/2$).[12] Therefore, the understanding of the role of e_g carriers with the variation of x—thus the collective phenomena of e_g carriers in connection with the specific kind of the charge ordering depending on x—has attracted great interest and may be a central topic in CO manganites. More recently, Asaka *et al.* proposed a model of the CE-type structure in $Pr_{0.625}Ca_{0.375}MnO_3$ by using transmission electron spectroscopy as schematically shown in Fig. 1(b).[13] It may be viewed as a quasi-one-dimensional electronic structure with reduced dimensionality as compared to the well-known CE-type structure [Fig. 1(a)]: $d_{3x^2-r^2}$ or $d_{3y^2-r^2}$ orbital ordering of Mn^{3+} occurs along the c axis. At another angle, the $d_{3z^2-r^2}$ orbital of Mn^{3+} was clipped by three Mn^{4+} ions. Such a regular pattern of the distinct charges modifies the uniformity of the charge density, leading to the development of the charge-density-wave (CDW) condensate.[14] This situation is depicted in Fig. 1(c); the charge density (shared area) periodically varies with the position and also time (dashed line),

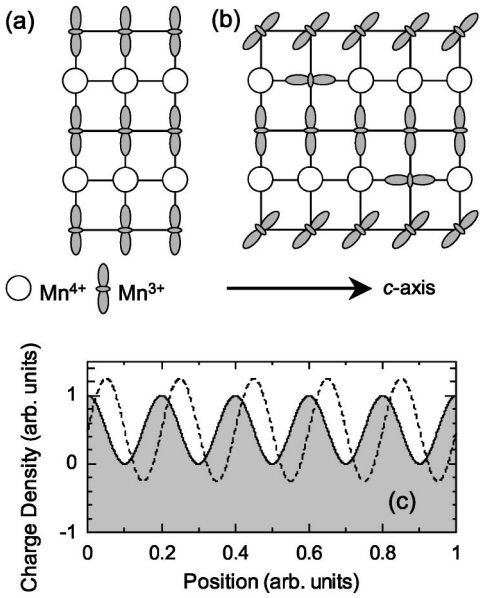

FIG. 1. Schematic arrangements of the (a) charge-exchange (CE)-type charge and orbital ordering pattern observed in half-doped manganites and (b) CE-type structure as proposed in $Pr_{0.625}Ca_{0.375}MnO_3$ along the c axis by Asaka *et al.* (Ref. 13). Pr and Ca atoms are omitted to clarify. (c) Schematic illustration of the charge-density-wave formation.

so the new modulation occurs in the underlying lattice (the period of this modulation is larger than the lattice constant). Such a CDW formation was recently deduced from the one-dimensional Fermi-surface (FS) topology in a layered manganite $La_{1.2}Sr_{1.8}Mn_2O_7$ by Chuang *et al.*;[15] they determined the detailed map of the FS by using angle-resolved photoemission spectroscopy and concluded that FS is subject to CDW instabilities even in the ferromagnetic metallic state. In slight of these considerations, the charge ordering is also characterized by a collective excitation well below 2Δ. However, no clear evidence for the collective excitation of the CO state was reported so far (see *Note added* at the end of the paper).

The collective excitation is associated with the mode depending on both the position and the time; the modes arising from the former and the latter are referred to as amplitudons and phasons, respectively.[16] According to Lee *et al.*,[17] the dispersion relation of the phasons is given by $\omega^2 \propto |q|^2$, where q is the wave number. By illumination of light, the collective excitation can make a coupled oscillation, which yields the change of the dielectric constant at $q=0$, being proportional to $(\omega_{\mathrm{LO}}^2-\omega^2)/(\omega_{\mathrm{TO}}^2-\omega^2)$, where ω_{LO} and ω_{TO} are the longitudinal and transverse optical frequencies, respectively. Therefore, this kind of coupled mode comes to the surface as a collective excitation mode in the complex optical spectrum. It is also important that the impurity and/or the lattice imperfection has a striking influence on the CDW dynamics, because the CDW condensate is pinned by the impurity and therefore the peak position of the collective excitation mode shifts to a finite frequency.[16]

In this article we provide spectroscopic evidence for the CDW condensate in the typical CO manganite $Pr_{0.7}Ca_{0.3}MnO_3$. The basis of this conclusion is derived from the first observation of the collective excitation mode in the optical conductivity spectrum. As in a well-known CDW system such as quasi-one-dimensional $K_{0.3}MoO_3$, the collective excitation mode frequently appears in the millimeter ω range $\sim$ meV,[16] where it is difficult to obtain the probing light by conventional optical spectroscopy. We overcome this limitation by using THz time-domain spectroscopy (TDS),[18] which is a powerful tool to reveal the low-energy charge dynamics of the CMR manganites.[19,20] In addition to this advantage, THz TDS is especially suited to capture the signal of the fluctuation phenomenon as the high-ω THz pulse is sensitive and matches the typical time scale of the charge fluctuation in a correlated electron system, which is realized by THz TDS experiments on underdoped $Bi_2Sr_2CaCu_2O_8$.[21]

The material we used in this work is the typical CO manganite, $Pr_{0.7}Ca_{0.3}MnO_3$ with an orthorhombically disordered three-dimensional structure. This material exhibits insulating behavior and undergoes charge[3,22] and orbital[3,23] ordering below $T_{\mathrm{CO/OO}} \sim 220$ K and the antiferromagnetic spin ordering below $T_{\mathrm{N}} \sim 140$ K. Due to the deviation of x from 1/2, at which the charge ordering is most stable, the extra electrons ($x<1/2$) occupy the Mn^{4+} site while maintaining the charge ordering [Fig. 1(b)]. The remarkable characteristics compared to other CO manganites are an admissibility of the charge ordering and the CMR effect, in which the dramatic variance of the resistance by more than 10 orders of magnitude was attained.[24,25] Therefore, various kinds of experimental results have accumulated to date.[2] It should be mentioned that there are various interpretaions of the low-temperature phase below 110 K: One is due to the coexistence of the ferromagnetic and antiferromagnetic phases proposed by Jirák *et al.*;[3] another is the canted antiferromagnetic phase (or the spin-glass phase) reported by Yoshizawa *et al.*[22] An intimate identification is beyond the scope of this study; however, we can say that magnetic properties of our samples are consistent with the results of Deac *et al.*[26]

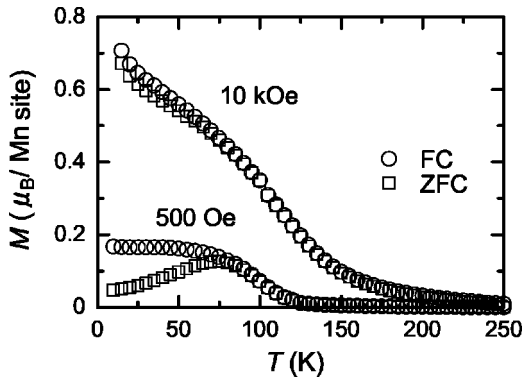

FIG. 2. Temperature T dependence of the magnetization M in a unit of Bohr magnetron μ_B at the Mn site of the sample A. Circles and squares represent $M(T)$ taken from the field cooling (FC) and zero-field cooling (ZFC) scans under the magnetic field of 500 Oe or 10 kOe, respectively.

II. METHODS

A. Sample preparation and characterization

$Pr_{0.7}Ca_{0.3}MnO_3$ thin films on MgO(100) substrates were prepared by a pulsed laser deposition technique using a KrF excimer laser (248 nm in the center wavelength). The thin films were deposited at 800 °C under an oxygen pressure $P(O_2)$ of 100 Pa and subsequently cooled down under $P(O_2)$ of 300 Pa. An x-ray diffraction pattern at room temperature indicates that the obtained films were of single phase and were mainly a (b) axis oriented in the cubic setting [we barely detected the (110) intensity peak in the logarithmic intensity scale]. We used two samples (A and B) in the following THz TDS experiments, both of which are obtained by the same growth condition described above. The film thickness d of the samples A and B are ~ 60 nm and ~ 100 nm, respectively. We measured the d dependence of the a (b)-axis lattice constant and observed its sudden increase above ~ 100 nm with the intense (110) intensity peak, implying the partial relaxation of the strained epitaxial growth below ~ 100 nm. The obtained films show typical insulating behavior between 20 and 300 K according to the dc resistivity $1/\sigma_1(\omega=0)$ measurements with a four-probe method.

To characterize magnetic properties of our samples, we measured T and H dependences of the magnetization M in units of the Bohr magnetron μ_B at the Mn site by a superconducting quantum interference device (SQUID) magneto-

TABLE I. Magnetic characteristics of the sample A deduced from Fig. 2 and the sample B at magnetic field $H=500$ Oe and 10 kOe: the temperature T_{irr} at which the temperature T dependence of the magnetization $M(T)$ in the field cooling (FC) and zero-field cooling (ZFC) scans deviate; $\Delta M=(M_{FC}-M_{ZFC})/M_{FC}$ at 15 K; and $\Delta T=T_{irr}-T_{max}$, where M_{FC} and M_{ZFC} are M in the FC and ZFC scans, respectively, and T_{max} is the maximum temperature in $M_{ZFC}(T)$.

	Sample A			Sample B		
H (Oe)	T_{irr} (K)	ΔM	ΔT (K)	T_{irr} (K)	ΔM	ΔT (K)
500	115	0.69	40	115	0.82	30
10 000	80	0.05[a]	65[a]	80	0.06[a]	65[a]

[a]Note, we define ΔM at 15 K and regard T_{max} as 15 K. In the original report of Deac *et al.* (Ref. 26), they used these values at 4 K.

meter. All data are collected by subtracting the contribution of M of the MgO substrates, which are measured independently. Figure 2 shows T dependence of M of the sample A in the field cooling (FC; open circles) M_{FC} and the zero-field cooling (ZFC; open squares) M_{ZFC} under 500 Oe or 10 kOe. With decreasing T for 500 Oe, both $M_{FC}(T)$ and $M_{ZFC}(T)$ curves are enhanced below 120 K and the $M_{ZFC}(T)$ curve starts to deviate from the $M_{FC}(T)$ curve below the irreversible temperature $T_{irr}\sim 80$ K. With further decreasing T, the $M_{ZFC}(T)$ curve reaches a maximum at temperature $T_{max}\sim 75$ K. The difference between M_{FC} and M_{ZFC} at 15 K is estimated to be $\sim 0.1\mu_B$ at the Mn site. On the other hand, $M_{FC}(T)$ and $M_{ZFC}(T)$ curves for 10 kOe are almost identical; we observed a continual increase of M_{ZFC} without the broad maximum and that the difference between M_{FC} and M_{ZFC} at 15 K is fairly small. The obtained magnetic properties of the samples A and B are listed in Table I together with $\Delta M=(M_{FC}-M_{ZFC})/M_{FC}$ at 15 K and $\Delta T=T_{irr}-T_{max}$. These quantities and behaviors of $M(T)$ curves both for 500 Oe and 10 kOe are consistent with previous detailed magnetic studies in single-crystal and ceramic samples of $Pr_{0.7}Ca_{0.3}MnO_3$ by Deac *et al.*[26] It is noted that we employ ΔM at 15 K and regard T_{max} as 15 K, while Deac *et al.* used these values at 4 K.

We show in Fig. 3 the M-H curve within ± 10 kOe at 30 K after T is decreased under zero H. The H cycling is changed (a) between -50 kOe and 50 kOe and (b) between -10 kOe and 10 kOe. There is a precursor signal of the metamagnetic transition due to the melting of the charge ordering in Fig. 3(a) in contrast to the M-H curve shown in Fig. 3(b):[24] M in the first increase H (closed circles) does not merge into M in the subsequent third increasing and second decreasing process (open circles); M steeply increases around 45 kOe. Once H exceeds the critical field around 45 kOe [inset of Fig. 3(a)], the magnitude of M in the subsequent increasing and decreasing process is larger than that shown in Fig. 3(b) (see M at -10 kOe).

We do not directly identify $T_{CO/OO}$ of our samples by, e.g., the transmission electron microscopy. However, as will be shown later, the T dependence of the optical conductivity

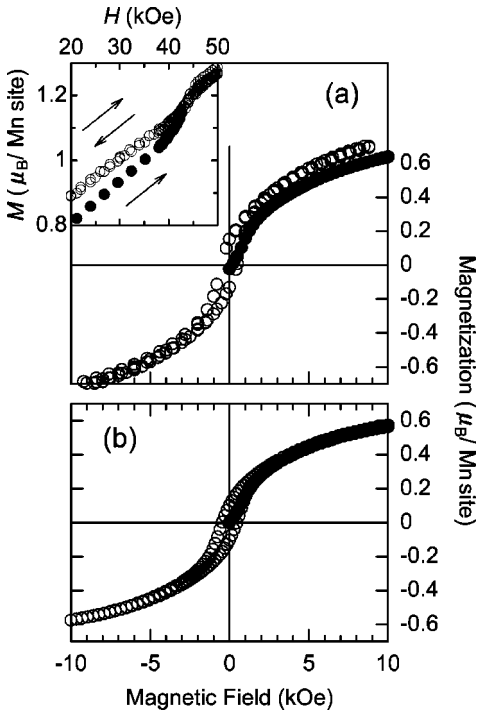

FIG. 3. Magnetization M in a unit of Bohr magnetron μ_B at the Mn site as a function of the magnetic field H of the sample A at 30 K. The H cycling is changed between (a) -50 kOe and 50 kOe and (b) -10 kOe and 10 kOe. $M(H)$ curve in the first increasing of H and $M(H)$ curve in third increasing and second decreasing of H are shown by closed and open circles, respectively. The inset of (a) shows an enlarged view around the metamagnetic transition.

changes around 220 K (see Fig. 6), which is nearly the same value of $T_{CO/OO}$ in this material (Ref. 3). Moreover, we recently found that the T dependence of THz radiation from the $Pr_{0.7}Ca_{0.3}MnO_3$ thin film, which is made by the same growth procedure in this work, dramatically changes at 140 K and 220 K.[27] Therefore we consider that our films have a $T_{CO/OO}$ around 220 K.

B. THz time-domain spectroscopy

We performed THz TDS experiments utilizing a photoconducting sampling technique in a transmission configuration. THz TDS experiments can directly provide complex optical spectra without the Kramers-Kronig transformation, which is an indispensable relation to estimate complex optical spectra using the conventional optical spectroscopy (reflection or transmission measurements as described in Sec. I). The principle of the THz TDS can be found in Refs. 18–20. We briefly describe the experimental setup of our THz TDS experiments. The light source is a THz pulse from a dipole-type low-temperature-grown GaAs (LT-GaAs) photoconducting switch under a voltage bias of 15 V excited by femtosecond optical pulses from the mode-locked Ti:sapphire laser (800 nm in the center wavelength, 150 fs in the pulse width). The THz pulse through the sample is detected by the bowtie-type LT-GaAs photoconducting switch. In the measured ω range, optical constants of the MgO substrate have negligible variation with respect to both ω and T.

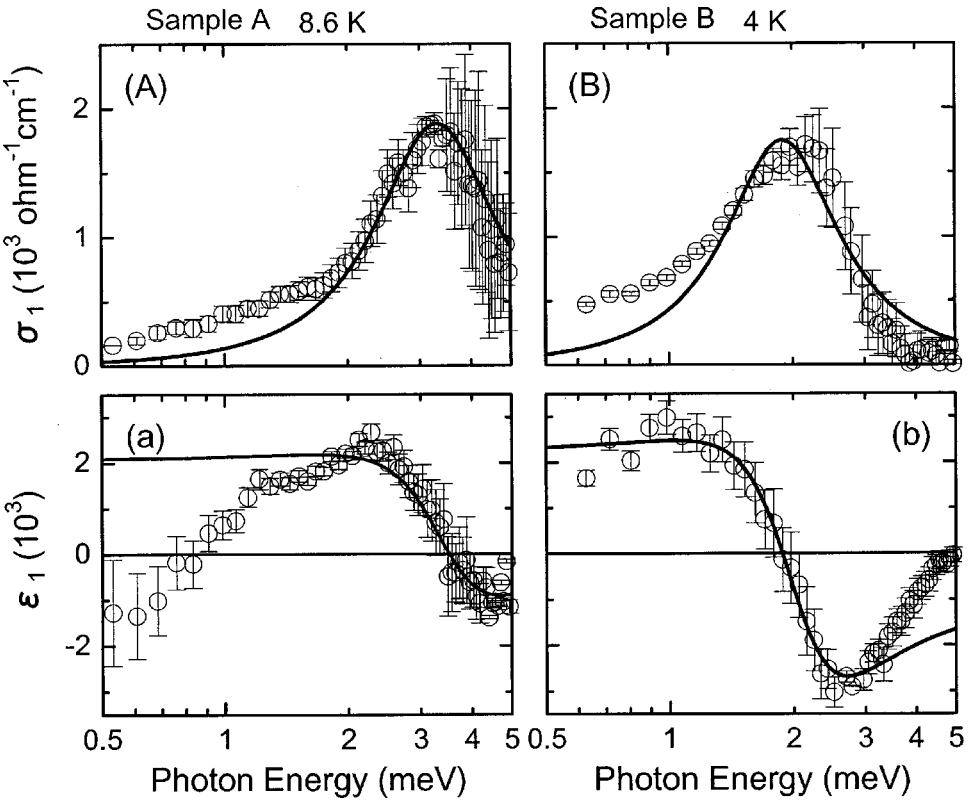

FIG. 4. Logarithmic energy plot of the real part of the complex optical conductivity spectrum $\sigma_1(\omega)$ of $Pr_{0.7}Ca_{0.3}MnO_3$ for (A) sample A and (B) sample B at 8.6 K and 4 K, respectively. The real part of the dielectric spectrum $\epsilon_1(\omega)$ of (a) sample A and (b) sample B are also shown in the lower panel of (A) and (B), respectively. Solid lines in $\sigma_1(\omega)$ and $\epsilon_1(\omega)$ represent fitting results to experimental data (open circles) using Eqs. (1) and (2) with parameters listed in Table II, respectively.

Therefore, we adopt the data of the MgO substrate at room temperature. By performing the Fourier transformation for the transmitted THz pulse, amplitude and phase shift spectra of $Pr_{0.7}Ca_{0.3}MnO_3$ thin films are obtained. We numerically estimated the complex refractive index spectrum $\tilde{n}(\omega) = n(\omega) - i\kappa(\omega)$ of $Pr_{0.7}Ca_{0.3}MnO_3$ (for the detailed procedure, see Ref. 19). Then, we transformed to the complex dielectric and complex optical conductivity spectra by using following relations: $\tilde{\epsilon}(\omega) = \epsilon_1(\omega) - i\epsilon_2(\omega) = n(\omega)^2 - \kappa(\omega)^2 - i2n(\omega)\kappa(\omega)$ and $\tilde{\sigma}(\omega) = \sigma_1(\omega) - i\sigma_2(\omega) = \epsilon_0\omega\{\epsilon_2(\omega) - i[\epsilon_\infty - \epsilon_1(\omega)]\}$, respectively, where ϵ_∞ is the dielectric constant of the bound electrons and ϵ_0 is the permittivity of vacuum.

III. RESULTS

Figures 4(A) and 4(B), respectively, show $\sigma_1(\omega)$ with a logarithmic energy scale of $Pr_{0.7}Ca_{0.3}MnO_3$ for two samples A and B at low temperature. We also plot in Figs. 4(a) and 4(b) $\epsilon_1(\omega)$ corresponding to $\sigma_1(\omega)$ of the samples A and B, respectively. The experimental configurations differ from each other, so the light source of the THz pulse is different in respective measurements. The open circles denote experimental data. The scattering of the data represented by error bars are large below 0.5 meV and above 4 meV due to a poor sensitivity of the THz light sources and an ambiguous convergence of the transformation procedure. There are important and striking features, which can be clearly seen in the

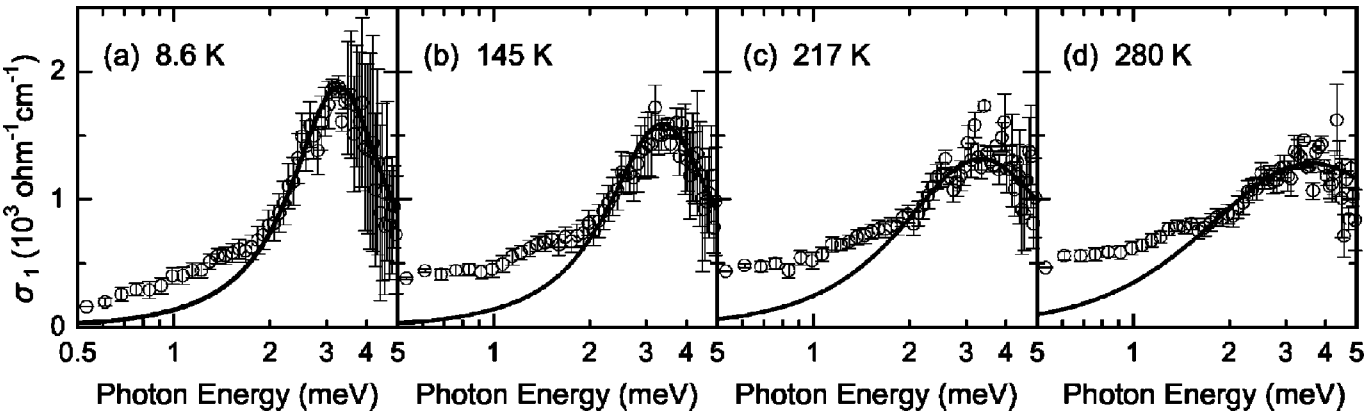

FIG. 5. Logarithmic energy plot of the real part of the complex optical conductivity spectrum $\sigma_1(\omega)$ of the sample A measured at (a) 8.6 K, (b) 145 K, (c) 217 K, and (d) 280 K. The data are taken from the temperature-warming run. Solid lines represent fitting results to experimental data (open circles) using Eq. (1).

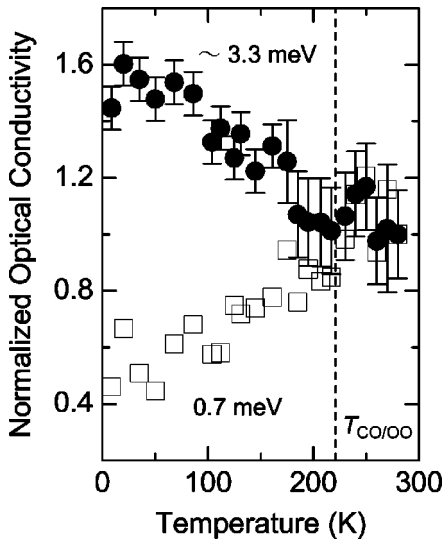

FIG. 6. Temperature dependence of the real part of the complex optical conductivity at the peak frequency (closed circles) and at 0.7 meV (open squares) of the sample A. The respective data are normalized by the value at 280 K. The dashed line represents the charge and orbital ordering temperature $T_{CO/OO}$.

measured ω range (0.5–5 meV): (i) a finite peak structure appears in $\sigma_1(\omega)$ centered around 2–3 meV below the lowest optical phonon energy ~20 meV (the external optical phonon mode originated from the perovskite structure[6]). Accordingly, the distinguished sharp peaks with a dispersive structure are observed in $\epsilon_1(\omega)$; the peak frequency in $\sigma_1(\omega)$ nearly corresponds to $\epsilon_1(\omega)=0$. (ii) The observed structure has a small spectral weight of the order of 1% as compared to the single-particle excitation;[5,6,9] $\sigma_1(\omega)$ at the peak frequency (~2000 Ω^{-1} cm^{-1}) bears comparison with that at ~1 eV (~1000 Ω^{-1} cm^{-1}). (iii) Its peak position strongly depends on samples, while $\sigma_1(\omega)$ at the peak frequency does not. (iv) The swelling of $\sigma_1(\omega)$ around 1 meV is observed below the finite peak structure. Conformably, $\epsilon_1(\omega)$ continues to exhibit ω dependence; in particular

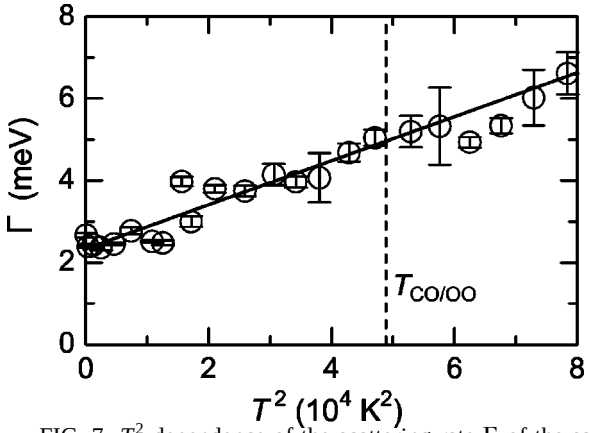

FIG. 7. T^2 dependence of the scattering rate Γ of the sample A deduced from Eq. (1). The data are taken from the *T*-warming run. The solid line denotes a fitting result to the data (open circles) using Eq. (3). The dashed line indicates the charge and orbital ordering temperature $T_{CO/OO}$.

TABLE II. The obtained quantities deduced from the fitting results to the data shown in Figs. 4 by Eqs. (1) and (2) for different samples A (at 8.6 K) and B (at 4 K); the peak frequency ω_0, the relaxation time τ, the scattering rate $\Gamma=1/\tau$, the optical conductivity σ_0 at ω_0, and the dielectric constant of the bound electrons ϵ_∞ .

Sample	ω_0 (meV)	τ (ps)	Γ (meV)	σ_0 (Ω^{-1} cm^{-1})	ϵ_∞
A	3.3	0.25	2.6	1880	150
B	1.9	0.45	1.9	1750	1000

$\epsilon_1(\omega)$ of the sample A cuts another zero around 0.8 meV.

To reveal the spectral shape of the finite peak structure with *T*, we performed the same experiments with sample A on warming through $T_{CO/OO}$~220 K; $\sigma_1(\omega)$ at selected *T* [(a) 8.6 K, (b) 145 K, (c) 217 K, and (d) 280 K] are shown in Fig. 5. Figure 5(a) is same as Fig. 4(A). With increasing *T* up to $T_{CO/OO}$, $\sigma_1(\omega)$ around the peak frequency decreases and the spectral shape broadens out, while the swelling structure increases [Figs. 5(b) and 5(c)]. Even above $T_{CO/OO}$, the peak structure is still visible [Fig. 5(d)]. One can notice that the spectral shape around the peak structure at 217 K [Fig. 5(c)] does not considerably change above $T_{CO/OO}$ as can be seen in that at 280 K [Fig. 5(d)]. In addition, the peak frequency does not depends on *T*.

To clarify the change of $\sigma_1(\omega)$ more clearly with *T*, we plot in Fig. 6 the *T* dependence of the $\sigma_1(\omega)$ at the peak frequency (closed circles) and at 0.7 meV (open squares) of sample A, which is normalized by the value of the respective $\sigma_1(\omega)$ at 280 K. It can be clearly seen that $\sigma_1(\omega)$ both at the peak frequency and at 0.7 meV above $T_{CO/OO}$ do not show *T* dependence within experimental accuracy [the data of $\sigma_1(\omega)$ around the peak structure are subject to the inaccuracy in the transformation procedure with increasing *T*. Thus, the scattering of the data is large]. In contrast, with decreasing *T* below $T_{CO/OO}$, $\sigma_1(\omega)$ at the peak frequency increases and reaches the maximum value at low temperature, which is 1.6 times larger than the value at $T_{CO/OO}$, while $\sigma_1(\omega)$ at 0.7 meV decreases slightly. These results clearly indicate that the observed structure is related to the opening of 2Δ.

IV. ASSIGNMENT AND DISCUSSION

Keeping features of the finite peak structure described in Sec. III in mind, let us focus our attention on the assignment of the observed structure. At finite *T*, thermal fluctuations in the order of k_BT (~1 meV at 10 K) as well as the presence of the impurity band play an important role in the measured ω range, where k_B is Boltzmann's constant; some hopping conduction of the thermally excited carriers within 2Δ screens in the underlying lattice and subsequently gives rise to a finite peak structure (Ref. 28). From this viewpoint, the *T* dependence of the scattering rate of the charge carriers in the hopping event follows an exponential *T* dependence.[29] To see quantitatively how the observed structure changes with *T*, we applied a single Lorentz oscillator expressed as

$$\sigma_1(\omega)=\frac{\sigma_0\omega^2/\tau^2}{(\omega_0^2-\omega^2)^2+\omega^2/\tau^2}, \qquad (1)$$

$$\epsilon_1(\omega)=\epsilon_\infty+\frac{\omega_p^2(\omega_0^2-\omega^2)}{(\omega_0^2-\omega^2)^2+\omega^2/\tau^2}, \quad (2)$$

where ω_0 is the peak frequency, τ is the relaxation time, σ_0 is $\sigma_1(\omega)$ at ω_0, and ω_p is the plasma frequency. The solid lines in Figs. 4 denote least-squares fits to the respective data. In this procedure, we determined the value of the peak frequency ω_0, where $\epsilon_1(\omega)$ crosses zero and then fixed the value of σ_0. Thus only τ is a fitting parameter in Figs. 4(A) and 4(B). We also estimate ϵ_∞ using only the above-determined values. The obtained quantities of samples A and B are summarized in Table II. As clearly seen in Figs. 4, we can reproduce $\sigma_1(\omega)$ and $\epsilon_1(\omega)$ by using, respectively, Eqs. (1) and (2) except for the energy region, where the swelling appears in $\sigma_1(\omega)$. Figure 7 displays a T-square plot of the scattering rate $\Gamma=1/\tau$ of the sample A below 280 K. We found that $\Gamma(T)$ obey the phenomenogical relation given by

$$\Gamma(T)=\Gamma_0+A_2T^2, \quad (3)$$

where A_2 is the coefficient and Γ_0 is Γ at 0 K. The solid line in Fig. 7 is a least-squares fit to the data below $T_{CO/OO}$; Eq. (3) holds well with $\Gamma_0=2.3$ meV and $A_2=0.5$ meV/K^2, providing a clear indication that $\Gamma(T)$ cannot be accounted for by thermal as well as variable range hopping conduction pictures of the carriers in the localized state.[30]

One may consider the phase separation (PS) picture[31]—the dynamical coexistence of the ferromagnetic metallic and CO insulating states,[32] which is thought to be a key feature of the CMR phenomena and indeed experimentally discussed in $Pr_{0.7}Ca_{0.3}MnO_3$.[26,33,34] Such PS as well as the presence of the disorder commonly seen in thin films using MgO substrates produces a finite peak structure as a result of the shifting of the Drude peak centered at $\omega=0$. Our samples show ferromagnetic order at low temperature; there is a significant hysteresis loop in M-H curve at 30 K with a coercive force of $\sim$500 Oe (Figs. 3), which may imply the presence of the ferromagnetic domain in the CO insulating phase. Therefore, we compare our experimental results to the typical characteristics of the PS in CO manganites.[34–36] The best example in the PS picture is the slow relaxation effect observed in $Pr_{0.67}Ca_{0.33}MnO_3$ by Anane *et al.* (Ref. 34) and Cr-doped manganites by Kimura *et al.*,[35] in which the ferromagnetic fraction can be artificially controlled by the H-annealing process and also Cr (impurity) doping at the Mn-site. In these materials, the physical quantities [i.e., $\sigma_1(\omega=0)$ and M] strongly depend on the history of the external perturbations. For example, Anane *et al.* measured the time dependence of $\sigma_1(\omega=0)$ in the ferromagnetic phase of $Pr_{0.67}Ca_{0.33}MnO_3$ after $H=100$ kOe is applied at low temperature.[34] They found that the CO insulating phase is restored in the time range of 10^2–10^5 s (the slow relaxation effect). Very recently, Mathieu *et al.* reported that M_{FC} at 20 Oe in $Nd_{0.5}Ca_{0.5}MnO_3$ exhibits a different relaxation effect in the typical characteristic time of $\sim10^2$ s by changing only the cooling rate.[36] Moreover, the difference of M_{FC} in the history of the cooling rate increases with time. Based on these studies, we have done following THz TDS experiments: We rapidly cooled the other sample used in Sec. III (the growth condition is same as samples A and B) from room temperature to 4 K with a cooling rate of ~8 K per minute and measured the time dependence of $\sigma_1(\omega)$ while keeping $T=4$ K constant. We observed no slow relaxation effect in the measured ω range; the spectral shape of the peak structure and the peak frequency ~2 meV exhibit no variation per $\sim10^4$ s, which is contrary evidence for the PS as an origin of the observed structure.

As described in Sec. I, we infer the possibility of the CDW condensate due to the quasi-one-dimensional charge and orbital ordering in $Pr_{0.7}Ca_{0.3}MnO_3$. We discuss here that the observed peak structure arises from the CDW condensate as compared to the low-energy optical properties of the well-known CDW system. The typical characteristics of the collective excitation mode observed in low-dimensional CDW materials are as follows:[16,37–41] (i) As mentioned earlier, the pinning frequency is in general of the order of meV.[16,37–41] (ii) The spectral weight of the collective excitation mode is typically two orders of magnitude smaller than that of the single-particle excitation.[16,37–41] This is due to the relatively large $2\Delta\sim100$ meV, which is in strong contrast to the small spin gap ~10 meV observed in the spin-density-wave (SDW) system. In the SDW system, the spectral weight of the collective excitation mode should be comparable to that of the single-particle excitation due to the electron-electron interaction.[42] (iii) Kim *et al.* found that the pinning frequency in $(Ta_{1-z}Nb_zSe_4)_2I$ alloys linearly shifts to higher ω and $\sigma_1(\omega)$ at the pinning frequency does not change with increasing the impurity concentration z.[39] Same tendencies are also observed in $K_{0.3}Mo_{1-z}W_zO_3$ alloys.[41] (iv) Mihály *et al.* identified the swelling structure in the low-energy side of the collective excitation mode in $K_{0.3}MoO_3$ as the internal deformation on the basis of the generalized Debye analysis.[38] Our present findings (i)–(iv) described in Sec. III and various works (i)–(iv) described above in the CDW system both have apparent similar properties and have no contradictions. Moreover, the T^2 dependence of Γ (Fig. 7) has been also found in the CDW system,[16,37] and Eqs. (1) and (2) are same expressions derived from the equation of motion for the CDW dynamics.[16] Therefore, we arrive at the conclusion that the observed structure in $Pr_{0.7}Ca_{0.3}MnO_3$ is assigned to the collective excitation mode arising from the CDW condensate.

The description of the CDW condensate in $Pr_{0.7}Ca_{0.3}MnO_3$ is consistent with and may help explain previous studies. The CDW easily couples with the lattice and affects phonon modes. Therefore, new infrared modes are expected to be active below $T_{CO/OO}$. Okimoto *et al.* found that in addition to phonon modes due to the orthorhombic distortion, many new modes emerge as sharp excitations in $Pr_{0.6}Ca_{0.4}MnO_3$ at 10 K.[6] Asamitsu *et al.* have measured current-voltage characteristics of $Pr_{0.7}Ca_{0.3}MnO_3$ and found the beginning of the nonlinear conduction above the threshold electric field,[43] which reminds us of the sudden motion of the CDW (CDW depinning) as observed in CDW materials.[16]

We should note previous work concerning the impurity effect on $\sigma_1(\omega)$ in a copper oxide superconductor. Basov *et al.* reported that the Zn (impurity) doping of the Cu site in

$YBa_2Cu_4O_8$ distracts the superconductivity and induced the finite peak structure around 10 meV (Ref. 44). They concluded that this structure arises from the localization of the charge carriers produced by the random distribution of Zn on the Cu site (disorder) on the basis that the integrated area of $\sigma_1(\omega)$ up to 1 eV conserves as much as 3.5% Zn doping. However, same authors also pointed out that if the Drude-like response in $YBa_2Cu_4O_8$ appears as a result of the collective excitation, which is predicted by theory, the peak structure in $YBa_2(Cu_{1-z}Zn_z)_4O_8$ can be regarded as the collective excitation mode as in both cases of the CDW and SDW.[44]

It is well known that the collective excitation mode originates in two different states; one is a ''pinned'' state due to the pinning of the CDW condensate by the impurity and/or the lattice imperfection and another is the ''bound'' state, which is created by the coupling of the pinned state with the optical phonon or the impurity near the pinned state.[40,41] Despite the fact that the swelling of $\sigma_1(\omega)$ below the low-energy side of the finite structure, which is usually ascribed to a internal deformation of the pinned collective excitation mode,[38] can be seen in Fig. 4, we cannot clearly claim whether the observed mode is assigned to the pinned or the bound collective excitation mode of the CDW. One possible result is that $\epsilon_1(\omega)$ below the peak structure crosses zero around 8 meV and reaches a negative value with decreasing ω [Fig. 4(a)]. This implies the presence of another ω_p and of another peak structure below the measured ω range. Further experiments on $\tilde{\sigma}(\omega)$ in the GHz ω range are necessary to obtain detailed data and are now in progress using the cavity perturbation technique.

As shown in Fig. 5(d), the collective excitation mode can be seen even above $T_{CO/OO}$, while its spectral shape is blurred due to the large proportion of the background contribution above $T_{CO/OO}$. Γ continues to follow a T^2 dependence above $T_{CO/OO}$ as shown in Fig. 7 [the fitting procedure by Eq. (3) was performed using the data below $T_{CO/OO}$]. This excludes thermal fluctuation as the origin of this broadening, leading us to conclude that the dynamical short-range CO (charge fluctuation) is still subsistent above $T_{CO/OO}$ instead of the long-range CO below $T_{CO/OO}$. Such a short-range CO has been already reported by other experiments: Radaeli *et al.* and Shimomura *et al.* have revealed that the short-range CO of $Pr_{1-x}Ca_xMnO_3$, with $x=0.3$,[33] 0.35, 0.4, and 0.5,[45] exists even above $T_{CO/OO}$ by neutron and x-ray scattering experiments, respectively. As in the case of a CDW system such as $K_{0.3}Mo_{1-z}W_zO_3$ and $(TaSe_4)_2I$, the collective excitation modes are also observed above the CDW transition temperature T_{CDW} due to the presence of the fluctuating CDW segments, which are systematically investigated by Schwartz *et al.*[46] For example, the collective excitation mode of $K_{0.3}MoO_3$ is visible even at 300 K ($T_{CDW} \sim 183$ K).

Finally, we comment on THz radiation from $Pr_{0.7}Ca_{0.3}MnO_3$ thin films excited by the femtosecond optical pulses, which we found recently;[27] the radiated spectrum decreases rapidly in intensity with increasing ω and seems to show the depletion around 2.4 meV. As compared to Fig. 4, such a THz response is due to the absorption of the collective excitation mode during the propagation of the generated THz pulse inside the material.

V. SUMMARY AND OUTLOOK

Summarizing, by using THz TDS, we reported the presence of a finite peak structure around 2–3 meV in $Pr_{0.7}Ca_{0.3}MnO_3$ and assigned it to the collective excitation mode arising from the CDW condensate. The measurements on the polarization dependence of $\sigma_1(\omega)$ with the grazing incidence of light using the single-domain single crystal will provide direct evidence and more detailed information for the collective excitation mode. In particular, the measurements of $\sigma_1(\omega)$ in the GHz ω range are needed to perform further quantitative investigations. Further plans are to study the melting process under external perturbations and x dependence of the collective excitation mode; for example, 2Δ decreases linearly with x from 0.3 to 0.5,[9] whereas $T_{CO/OO}$ gradually increases and behaves in a less x-dependent way.[25] This indicates the breaking of the BCS relation given by $2\Delta(x) \propto T_{CO/OO}(x)$. Therefore, it is indispensable to clarify how the collective excitation mode manifesting well below 2Δ changes with x using THz TDS.

Note added. Recently, we became an aware of some reports related in the present study. Kitano *et al.*[47] and Gorshunov *et al.*[48] found peak structures around 0.1–1 meV in spin-ladder material $Sr_{14-x}Ca_xCu_{24}O_{41}$ by means of optical spectroscopy and assigned them to the collective excitation modes due to the CDW formation. Concerning manganites, Campbell *et al.*[49] interpreted that CDW fluctuations are inherent in a layered ferromagnetic manganite $La_{1.2}Sr_{1.8}Mn_2O_7$ based on their diffuse x-ray scattering data. Recently, Nagai *et al.*[50] reported that the electron microscopic data of a layered CO manganite $Nd_{1-x}Sr_{1+x}MnO_4$ are consistent with assumptive images of CDW formation. Very recently, the finite peak structure around 4 meV was also found in 1/8 hole-doped $La_{1.275}Nd_{0.6}Sr_{0.125}CuO_4$ by Dumm *et al.*[51] as in the case of $YBa_2(Cu_{1-z}Zn_z)_4O_8$. They also ascribe this structure to the localization of the charge carriers in the static stripe phase due to the lack of 2Δ in this material. However, Fujita *et al.*[52] reported evidence for CDW and SDW formations in 1/8 hole-doped $La_{1.875}Ba_{0.125-x}Sr_xCuO_4$ by elastic neutron scattering experiments.

ACKNOWLEDGMENTS

We would like to thank in particular Y. Okimoto and also K. Miyano, Y. Ogimoto, K. Takenaka, and Y. Tokura for giving fruitful comments and discussions. We are also grateful to T. Kawai for giving us the opportunity of using the SQUID apparatus, to T. Kanki, I. Kawayama, K. Takahashi, and H. Tanaka for their help with SQUID measurements, and to M. Misra for reading the manuscript.

[1] For a review of the transition metal oxides, see, M. Imada, A. Fujimori, and Y. Tokura, Rev. Mod. Phys. **70**, 1039 (1998).
[2] *Colossal Magnetoresistive Oxides*, edited by Y. Tokura (Gordon and Breach, New York, 2000).
[3] Z. Jirák, S. Krupička, Z. Šimša, M. Dlouhá, and S. Vratislav, J. Magn. Magn. Mater. **53**, 153 (1985).
[4] For a review of the optical properties of the manganites, see, Y. Okimoto and Y. Tokura, J. Supercond. **13**, 271 (2000).
[5] Y. Okimoto, Y. Tomioka, Y. Onose, Y. Otsuka, and Y. Tokura, Phys. Rev. B **57**, R9377 (1998).
[6] Y. Okimoto, Y. Tomioka, Y. Onose, Y. Otsuka, and Y. Tokura, Phys. Rev. B **59**, 7401 (1999).
[7] P. Calvani, G. De Marzi, P. Dore, S. Lupi, P. Maselli, F. D'Amore, S. Gagliardi, and S.-W. Cheong, Phys. Rev. Lett. **81**, 4504 (1998).
[8] H. L. Liu, S. L. Cooper, and S.-W. Cheong, Phys. Rev. Lett. **81**, 4684 (1998).
[9] T. Tonogai, T. Satoh, K. Miyano, Y. Tomioka, and Y. Tokura, Phys. Rev. B **62**, 13 903 (2000).
[10] Y. Tokura and N. Nagaosa, Science **288**, 462 (2000).
[11] E. Saitoh, S. Okamoto, K. T. Takahashi, K. Tobe, K. Yamamoto, T. Kimura, S. Ishihara, S. Maekawa, and Y. Tokura, Nature (London) **410**, 180 (2001).
[12] S. Mori, C. H. Chen, and S.-W. Cheong, Nature (London) **392**, 473 (1998).
[13] T. Asaka, S. Yamada, S. Tsutsumi, C. Tsuruta, K. Kimoto, T. Arima, and Y. Matsui, Phys. Rev. Lett. **88**, 097201 (2002).
[14] G. Grüner, *Density Waves in Solids* (Addison-Wesley, Reading, MA, 1994).
[15] Y.-D. Chuang, A. D. Gromko, D. S. Dessau, T. Kimura, and Y. Tokura, Science **292**, 1509 (2001).
[16] For a review of the CDW dynamics, see, G. Grüner, Rev. Mod. Phys. **60**, 1129 (1988).
[17] P. A. Lee, T. M. Rice, and P. W. Anderson, Solid State Commun. **14**, 703 (1974).
[18] M. C. Nuss and J. Orenstein, in *Millimeter and Submillimeter Wave Spectroscopy of Solids*, edited by G. Grüner (Springer-Verlag, Berlin, 1998), pp. 7–50.
[19] N. Kida, M. Hangyo, and M. Tonouchi, Phys. Rev. B **62**, R11 965 (2000).
[20] N. Kida and M. Tonouchi, in *Physics in Local Lattice Distortions*, edited by H. Oyanagi and A. Bianconi (American Institute of Physics, New York, 2001), pp. 366–370.
[21] J. Corson, R. Mallozzi, J. Orenstein, J. N. Eckstein, and I. Bozovic, Nature (London) **398**, 221 (1999).
[22] H. Yoshizawa, H. Kawano, Y. Tomioka, and Y. Tokura, Phys. Rev. B **52**, R13 145 (1995).
[23] M. v. Zimmermann, J. P. Hill, D. Gibbs, M. Blume, D. Casa, B. Keimer, Y. Murakami, Y. Tomioka, and Y. Tokura, Phys. Rev. Lett. **83**, 4872 (1999).
[24] Y. Tomioka, A. Asamitsu, Y. Moritomo, and Y. Tokura, J. Phys. Soc. Jpn. **64**, 3626 (1995).
[25] Y. Tomioka, A. Asamitsu, H. Kuwahara, Y. Moritomo, and Y. Tokura, Phys. Rev. B **53**, R1689 (1996).
[26] I. G. Deac, J. F. Mitchell, and P. Schiffer, Phys. Rev. B **63**, 172408 (2001).
[27] N. Kida and M. Tonouchi, Appl. Phys. Lett. **78**, 4115 (2001).
[28] D. Romero, S. Liu, H. D. Drew, and K. Ploog, Phys. Rev. B **42**, 3179 (1990).
[29] S. Liu, K. Karrai, F. Dunmore, H. D. Drew, R. Wilson, and G. A. Thomas, Phys. Rev. B **48**, 11 394 (1993).
[30] It is worth noticing that the appearance of the finite peak structure is a common feature in the disordered system but only in *conductors* near the compositional insulator-metal phase boundary. In general, the characteristic energy scale of the localized state in the impurity-doped *conducting* manganites, i.e., Al (impurity) doping at the Mn site of $La_{0.825}Sr_{0.175}MnO_3$ [K. Takenaka, Y. Sawaki, and S. Sugai, J. Phys. Soc. Jpn. **70**, 1896 (2001)] is about 100 meV, which is considerably different from the peak position of the observed structure.
[31] M. Mayr, A. Moreo, J. A. Vergés, J. Arispe, A. Feiguin, and E. Dagotto, Phys. Rev. Lett. **86**, 135 (2001).
[32] M. Uehara, S. Mori, C. H. Chen, and S.-W. Cheong, Nature (London) **399**, 560 (1999).
[33] P. G. Radaelli, R. M. Ibberson, D. N. Argyriou, H. Casalta, K. H. Andersen, S-W. Cheong, and J. F. Mitchell, Phys. Rev. B **63**, 172419 (2001).
[34] A. Anane, J.-P. Renard, L. Reversat, C. Dupas, P. Veillet, M. Viret, L. Pinsard, and A. Revcolevschi, Phys. Rev. B **59**, 77 (1999).
[35] T. Kimura, Y. Tomioka, R. Kumai, Y. Okimoto, and Y. Tokura, Phys. Rev. Lett. **83**, 3940 (1999).
[36] R. Mathieu, P. Nordblad, A. R. Raju, and C. N. R. Rao, Phys. Rev. B **65**, 132416 (2002).
[37] T. W. Kim, D. Reagor, G. Grüner, K. Maki, and A. Virosztek, Phys. Rev. B **40**, 5372 (1989).
[38] G. Mihály, T. W. Kim, and G. Grüner, Phys. Rev. B **39**, 13 009 (1989).
[39] T. W. Kim, S. Donovan, G. Grüner, and A. Philipp, Phys. Rev. B **43**, 6315 (1991).
[40] L. Degiorgi, B. Alavi, G. Mihály, and G. Grüner, Phys. Rev. B **44**, 7808 (1991).
[41] L. Degiorgi and G. Grüner, Phys. Rev. B **44**, 7820 (1991).
[42] For a review of the SDW dynamics, see, G. Grüner, Rev. Mod. Phys. **66**, 1 (1994).
[43] A. Asamitsu, Y. Tomioka, H. Kuwahara, and Y. Tokura, Nature (London) **388**, 50 (1997).
[44] D. N. Basov, B. Dabrowski, and T. Timusk, Phys. Rev. Lett. **81**, 2132 (1998).
[45] S. Shimomura, T. Tonegawa, K. Tajima, N. Wakabayashi, N. Ikeda, T. Shobu, Y. Noda, Y. Tomioka, and Y. Tokura, Phys. Rev. B **62**, 3875 (2000).
[46] A. Schwartz, M. Dressel, B. Alavi, A. Blank, S. Dubois, G. Grüner, B. P. Gorshunov, A. A. Volkov, G. V. Kozlov, S. Thieme, L. Degiorgi, and F. Lévy, Phys. Rev. B **52**, 5643 (1995).
[47] H. Kitano, R. Inoue, T. Hanaguri, A. Maeda, N. Motoyama, M. Takaba, K. Kojima, H. Eisaki, and S. Uchida, Europhys. Lett. **56**, 434 (2001).
[48] B. Gorshunov, P. Haas, T. Rõõm, M. Dressel, T. Vuletic, B. Hamzic, S. Tomic, J. Akimitsu, and T. Nagata, cond-mat/0201413 (unpublished).
[49] B. J. Campbell, R. Osborn, D. N. Argyriou, L. Vasiliu-Doloc, J. F. Mitchell, S. K. Sinha, U. Ruett, C. D. Ling, Z. Islam, and J. W. Lynn, Phys. Rev. B **65**, 014427 (2002).
[50] T. Nagai, T. Kimura, A. Yamazaki, T. Asaka, K. Kimoto, Y. Tokura, and Y. Matsui, Phys. Rev. B **65**, 060405(R) (2002).
[51] M. Dumm, D. N. Basov, S. Komiya, Y. Abe, and Y. Ando, Phys. Rev. Lett. **88**, 147003 (2002).
[52] M. Fujita, H. Goka, K. Yamada, and M. Matsuda, Phys. Rev. Lett. **88**, 167008 (2002).